Brain Struct Funct
DOI 10.1007/s00429-016-1329-3

ORIGINAL ARTICLE

Commonly preserved and species-specific gyral folding patterns across primate brains

Xiao Li[1] · Hanbo Chen[2] · Tuo Zhang[1,5] · Xiang Yu[1] · Xi Jiang[2] · Kaiming Li[3,7] · Longchuan Li[4] · Mir Jalil Razavi[6] · Xianqiao Wang[6] · Xintao Hu[1] · Junwei Han[1] · Lei Guo[1] · Xiaoping Hu[3] · Tianming Liu[2]

Received: 3 March 2016 / Accepted: 18 October 2016

Abstract Cortical folding pattern analysis is very important to understand brain organization and development. Since previous studies mostly focus on human brain cortex, the regularity and variability of cortical folding patterns across primate brains (macaques, chimpanzees and human) remain largely unknown. This paper presents a novel computational framework to identify common or unique gyral folding patterns in macaque, chimpanzee and human brains using magnetic resonance imaging (MRI) data. We quantitatively characterize gyral folding patterns via hinge numbers with cortical surfaces constructed from MRI data, and identify 6 common three-hinge gyral folds that exhibit consistent anatomical locations across these three species as well as 2 unique three hinges in macaque, 6 ones in chimpanzee and 14 ones in human. A novel morphology descriptor is then applied to classify three-hinge gyral folds, and the increasing complexity is identified among the species analyzed. This study may provide novel insights into the regularity and variability of the cerebral cortex from developmental perspective and may potentially facilitate novel neuroimage analyses such as cortical parcellation with correspondences across species in the future.

Keywords Cortical folding · Primate brains · Magnetic resonance imaging · Three hinges

X. Li, H. Chen and T. Zhang are co-first authors.

X. Hu and T. Liu are joint corresponding authors.

✉ Tianming Liu
tliu@cs.uga.edu

Xiaoping Hu
xhu@engr.ucr.edu

[1] School of Automation, Northwestern Polytechnical University, Xi'an, China

[2] Cortical Architecture Imaging and Discovery Lab, Department of Computer Science and Bioimaging Research Center, The University of Georgia, Athens, GA, USA

[3] Department of Bioengineering, UC Riverside, Riverside, GA, USA

[4] Marcus Autism Center, Emory University, Atlanta, GA, USA

[5] Brain Decoding Research Center, Northwestern Polytechnical University, Xi'an, China

[6] College of Engineering, The University of Georgia, Athens, GA, USA

[7] Present Address: West China Hospital of Sichuan University, Chengdu, China

Introduction

Convoluted cortical folding pattern successively emerges and delineate neocortex into gyri and sulci during brain development in most mammals with large brains. Since crucial information of brain development (Dubois et al. 2008; Giedd and Rapoport 2010; Li et al. 2014), cytoarchitecture (Fischl et al. 2008; Heimann and Meinzer 2009), and normal/abnormal cognitive functioning (Thompson et al. 2004; Tortori-Donati et al. 2005; Bullmore and Sporns 2009; Honey et al. 2010) were shown to be embedded in cortical folds, both the regularity and the variability of cortical folding pattern are of great research interest. For example, abnormal cortical folding has been associated with neurodevelopmental disorders such as lissencephaly (Landrieu et al. 1998), polymicrogyria (Barkovich 2010), schizophrenia (Sallet et al. 2003; Harris et al. 2004), and autism (Hardan et al. 2004; Harris et al. 2004; Nordahl et al. 2007). As the emerging of cortical folds was shown to be influenced by multiple neurogenesis progress

Published online: 31 October 2016

such as neuron wiring (Van Essen 1997; Nie et al. 2012) and cortical expansion (Richman et al. 1975), its complexity is also suggested to be a good indicator of brain maturation (Dubois et al. 2008; Giedd and Rapoport 2010) and neurodegenerative processes (Rosas et al. 2002; King et al. 2010; Pereira et al. 2012). Therefore, quantitative representation of cortical folding complexity (Zilles et al. 1988; Luders et al. 2006; Yu et al. 2006; Li et al. 2010) is of fundamental importance for the future understanding of brain functional architecture (Schoenemann 2006; Honey et al. 2009; Liu 2011) and the underlying mechanism that regulates neocortex convolution (Welker 1990; Van Essen 1997; Toro and Burnod 2005; Hilgetag and Barbas 2006; Nie et al. 2012; Bayly et al. 2014).

From the perspective of interspecies brain analysis, to understand the mechanism of human brain, macaque and chimpanzee are often selected as a model system (Rilling and Insel 1999; Passingham 2009). To compare and correlate brain functions across species, correspondence between brain anatomy and functional map is first needed. To establish interspecies correspondence, one strategy is to correlate functional networks detected by functional magnetic resonance imaging (fMRI) (Passingham 2009). For example, the default mode network, which has been well identified in human brain as an activity decreased network during task states (Greicius et al. 2003) has been reproducibly identified in macaque brain (Mantini et al. 2011). However, due to the limited availability of fMRI data, most studies still rely on cortical morphology to establish correspondence. For instance, based on surface representation, Van Essen and his colleagues have successfully established anatomy and functional correspondence between macaque brain and human brain in visual cortex (Van Essen 2002) and cerebellar cortex (Van Essen et al. 2001). For such purpose, reliable brain morphology descriptor that can capture and establish interspecies and intersubject correspondence is also of great demand.

However, the brain morphology of human, chimpanzee, and macaque brains are different in many ways, which makes it challenging to establish reliable correspondence. Besides the obvious differences in brain size, allometric analysis also showed that human brain is not simply allometrically scaled version of other anthropoid brains (Rilling 2006; Smaers and Soligo 2013). For example, the human brain is still 4.8 times the size of the monkey brain even if we scaled the brain size by body weight (MacLeod et al. 2003) and the size of human brain neocortex and temporal lobe are larger-than-expected in comparison with other primates (Rilling 2006). Nevertheless, in spite of the challenges, the interspecies differences create a valuable chance to investigate brain functional mechanism (Rilling and Seligman 2002; Barton 2006; Dunbar and Shultz 2007). Since the specialization of brain organization could be related to the specialization of brain functions, species-specific cortical folding pattern may tell us potential explanation of the specific capability of a species.

Facing previously discussed demands, a desired cortical folding pattern descriptor should be able to quantify the complexity, the regularity, and the variability of cortical convolution simultaneously. In previous studies, two major streams of descriptors have been proposed by far to model and represent cortical folding patterns, which is a multi-scale phenomenon (Li et al. 2010). One is based on the local-scale descriptor of curvature and its derivations (Neal et al. 2007), which identifies the small neighborhood of the examined cortical foci. Another is a global one. For instance, gyrification indices (GI) (Zilles et al. 1988; Hardan et al. 2004), spherical wavelets (Yeo et al. 2008), and intrinsic curvature (Ronan et al. 2013) were applied to analyze the folding pattern of the entire cortical surface or a certain lobe. However, most of these descriptors focus on quantifying cortical complexity. It is difficult to quantify the variation of folding patterns and infer anatomy correspondence of the cortical landscapes based on those excessively local-scale and global-scale descriptors.

Therefore, in this study, we adopt a meso-scale descriptor—hinge-based gyral representation—to represent cortical folding patterns and analyze the regularity and variability of cortical folds across human, chimpanzee, and macaque brain. The hinge-based descriptor is initially proposed in our previous work to study human brain (Li et al. 2010; Chen et al. 2014). In brief, this is a hybrid parametric and profiling method in the sense that it combines the advantages of both parametric method (achieving compact representation of morphology pattern) and profiling method (achieving flexibility of arbitrary morphology representation). We particularly focus on the gyral region where more than one gyral crests joint, namely three-hinge gyral folds, as they are relatively easier to identify without ambiguity and can better serve as a meso-scale anatomical landmarks. In addition, they are the linkages of gyral systems from multiple directions, such that they could be a proxy of the overall cortical folding landscape as well. In practice, we developed a novel computational framework to identify common three-hinge gyral folding patterns across primate brains based on MRI data. Then, a novel morphology descriptor was applied to further quantitatively analyze folding pattern of three-hinge gyral folds by classifying them into the combination of five basic folding types (Yu et al. 2013) and quantify the level of convolution complexity among the three species. In addition, the cortical folds that uniquely appear in certain species were also identified. The comparative study based on the quantified folding patterns can shed light on brain functional differences across primates and specialization of the human brain and the three-hinge gyral fold descriptor presents a new metric for brain development studies.

Methods

Neuroimaging data and pre-processing

Human brain imaging

64 human brains from the Q1 release of WU-Minn Human Connectome Project (HCP) consortium (Van Essen et al. 2012) were used in this study. The T1-weighted structural MRI had voxels with 0.7-mm isotropic, three-dimensional acquisition, T1 = 1000 ms, TR = 2400 ms, TE = 2.14 ms, flip angle = 8°, image matrix = 260 × 311 × 260. Pre-processing included brain skull removal and tissue segmentation via *FSL 2.0* (Jenkinson et al. 2012). To facilitate the comparison and analysis, all subjects were aligned to the same space of randomly selected template human subjects by flirt 6.0 in FSL (Jenkinson and Smith 2001; Jenkinson et al. 2002). Cortical surface reconstruction was then performed to reconstruct inner cortical surface of white matter (WM) (Liu et al. 2008).

Chimpanzee brain imaging

The chimpanzees were from a colony in the Yerkes National Primate Research Center (YNPRC) at Emory University in Atlanta, Georgia. All imaging studies were approved by the IACUC of Emory University. Prior to scanning, the subjects were immobilized with ketamine injections (2−6 mg/kg, i.m.) and were subsequently anesthetized with an intravenous propofol drip (10 mg/kg/h) according to standard veterinary procedures used at YNPRC. The subjects remained sedated for the duration of the scans as well as the time needed for transportation between their home cage and the scanner location. After completing scans, chimpanzees were temporarily housed in a single cage for 6–12 h to allow effects of anesthesia to wear off before being returned to their home cage and cage mates. The veterinary staff and research staff assessed the general well-being (i.e., activity, food intake) of the chimpanzees twice daily after the scan for possible distress associated with aesthetic accesses. T1-weighted MRI scans obtained from 16 adult female chimpanzees were used for this study.

The pre-processing is similar to human brain data which include skull removal, tissue segmentation, WM cortical reconstruction, and linear registration to the template space of a randomly selected subject. Since we will not compare the brain volume size in this paper and some of the methods proposed are sensitive to the size of brain, we scaled the chimpanzees' brain to the same size as human brain.

Macaque brain imaging

The macaque subjects were members of a colony at YNPRC. All scans were approved by IACUC of Emory University. Prior to scanning, the subjects were immobilized with ketamine injections (2–6 mg/kg, i.m.) and were subsequently anesthetized with an intravenous propofol drip (10 mg/kg/h) following standard veterinary procedures used at YNPRC. The macaques remained sedated for the duration of the scans as well as the time needed for transportation between their home cage and the scanner location. After completing scans, macaques were temporarily housed in a single cage for 6–12 h to allow the effects of anesthesia to wear off before being returned to their home cage and cage mates. The veterinary staff and research staff observed the general well-being (i.e., activity, food intake) of the macaques twice daily after the scan for possible distress associated with anesthetic accesses. T1-weighted MRI data from 20 subjects were used for this study. The pre-processing is similar to human brain data which include skull removal, tissue segmentation, WM cortical reconstruction, linear registration to the template space of a randomly selected subject, and scaling to the same size as human brain.

Three-hinge gyral fold extraction

In this work, we adopted the methodology of describing cortical gyral folding patterns via hinge numbers (Li et al. 2010; Chen et al. 2014). Basically, a gyral hinge was defined as the region at the top of gyrus with the maximal folding curvature. When connecting hinges along a gyral crest, a gyral hinge curve could be traced. When multiple hinge curves encountered at a cross-point, the number of hinge curves connecting to this cross-point could be used to characterize and describe folding pattern of this gyrus (Fig. 1) (Li et al. 2010). To automatically identify cross-point vertices of the three-hinge folds, we adopted and adjusted the method proposed in our previous work (Li et al. 2010). The method was initially designed to profile cortical folding in human brain. We adjusted the method to make it more precise and flexible for both macaque brain and chimpanzee brain. We first profiled on each vertex on the surface to get features of each vertex and then we did second profiling on the corresponding inflated surface to find three-hinge centers.

First profile (Fig. 2a–d)

First, all vertices on the surface need to be classified into two groups, gyri and sulci. Here, we briefly introduce the

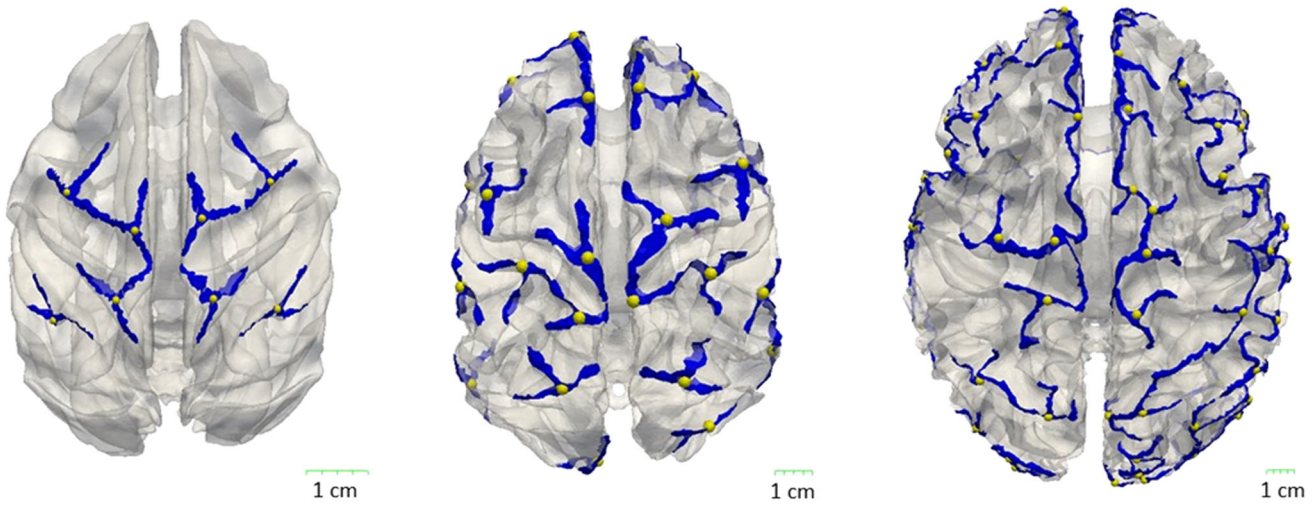

Fig. 1 Illustration of three-hinge gyral folds in three species (from *left to right* are macaque, chimpanzee and human brain, respectively). A three-hinge gyral fold consists of three hinges along the connected cortical gyri and their junction (the *yellow spheres* in Fig. 1). It can be seen that the cortical surfaces of human brain and chimpanzee brain are more convoluted than that of macaque brain, and that the three-hinge gyral folds are more symmetrically distributed in chimpanzee brain and macaque brain in comparison with human brain

method (Li et al. 2010) to profile and extract features of each vertex on the whole surface. A 3D coordinate system was built for every vertex on the cortical surface, as there exists a normal direction as the Z direction, as well as a tangent plane represented by a 2D polar coordinate system. The initial direction in the polar coordinate system was randomly selected. Then we sampled every vertex's surface patch into 72 evenly distributed spokes (5 degree interval) from the initial direction (Fig. 2b). Each spoke was 20 mm long and 20 points were evenly sampled along it. After that a power function was applied to fit the model of each spoke:

$$y = b + y_0(x/x_0)^n \quad (1)$$

Here, (x, y) is the 2D Cartesian coordinate of a profile according to the 2D polar coordinate system; x_0, y_0, n, b are parameters to describe a profile. The parameters of this model were evaluated in a least-square sense with Levenberg–Marquardt algorithm (Marquardt 1963) and the values of these parameters could be used to extract features of any vertex on the surface. These features include average ratio, average concave, average convex and sulci or gyri. Average ratio measures the average ratio between y_0 and x_0 of all samples. Average concave measures the average ratio between y_0 and x_0 for all profiles that correspond to local minima at the ratio curve, while average convex corresponds to local maxima at the ratio curve. Sulci or gyri classify one vertex to a sulci vertex or a gyri vertex according to the result whether it had more profile points below its tangent plane (Fig. 2c). With these extracted features, we can classify each vertex into two categories: gyri or sulci (Fig. 2d).

Second profile (Fig. 2e–i)

Then, an inflated surface was generated by FreeSurfer (Fischl et al. 1999) without changing the surface topology such as the number of vertices and gyro-sulcus patterns, and the correspondence between inflated surface and original surface retains (Fig. 2d, f). The second profile of each point was then generated on the inflated surface. For each cortical vertex, the profile process was the same as the first profile on the origin surface with 72 evenly distributed spokes (5 degree interval) (Fig. 2g). Each spoke was 20 mm long and 20 points were evenly sampled along it. Each point was projected onto the inflated surface and could be classified to gyri or sulci group. Our goal is to identify three hinges on gyri; therefore, only the profiles of vertices on gyri are considered (blue dots in Fig. 2h). Then the spokes were classified into two types—either all points are on gyri or only part of them is on gyri. For the profile of a vertex, the adjacent all-gyri spokes were clustered into a group and the vertex involving three all-gyri spoke groups was taken as three-hinge vertex. Finally, we clustered the adjacent three-hinge vertices and each cluster was taken as three hinges. The vertex closest to the center of the cluster was taken as the center vertex of three hinges (Fig. 2i).

Morphology descriptor of three-hinge gyral fold

We applied our prior method (Yu et al. 2013) to describe gyral folding patterns of each three-hinge fold by describing single hinge with five basic morphology patterns. For each three-hinge fold, a local coordinate system

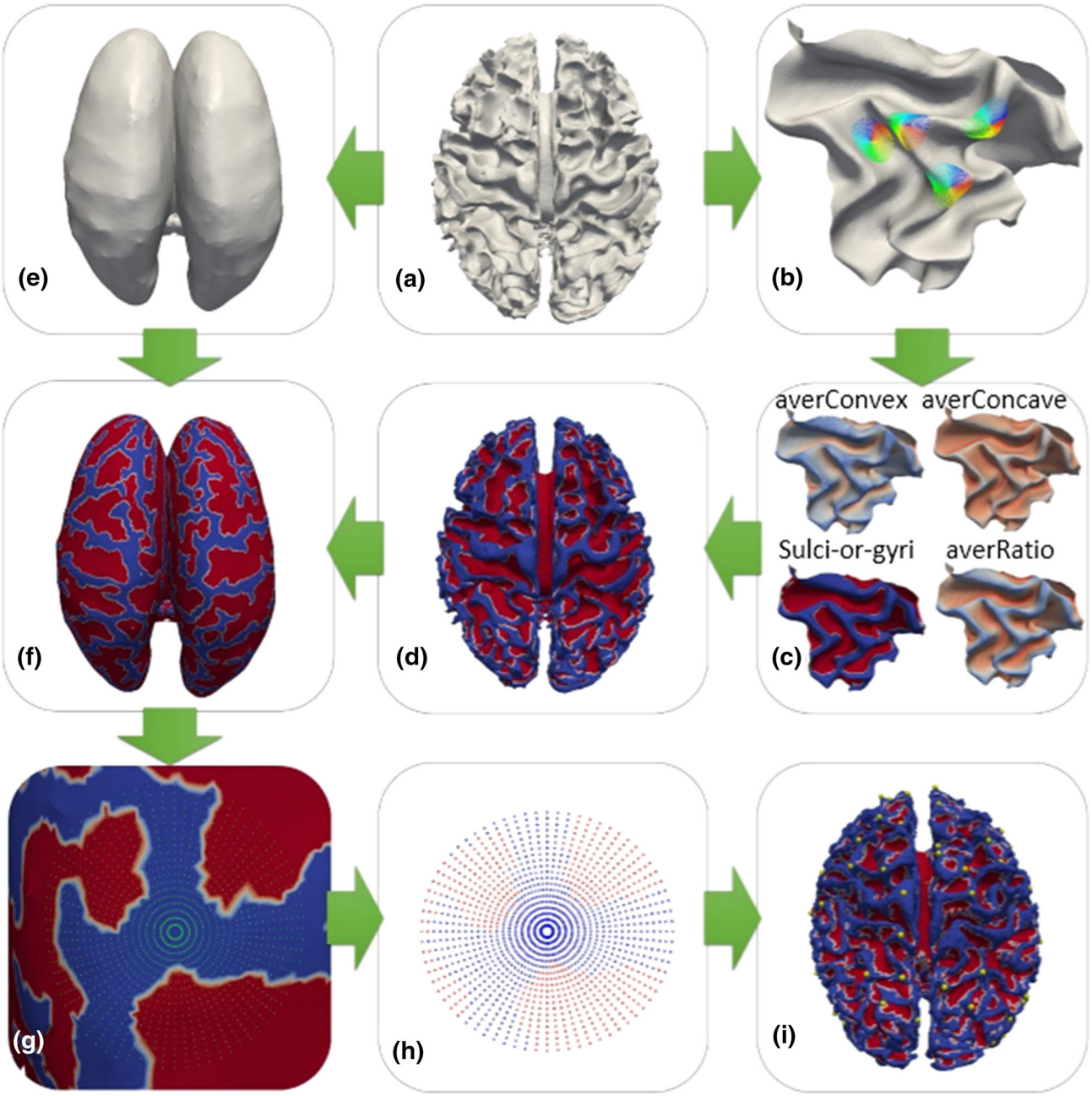

Fig. 2 Illustration of automatic three-hinge gyral fold extraction. **a** A reconstructed WM cortical surface. **b** Profiling every voxel on the surface. **c** Cortical features detected after profiling. **d** The cortical surface profiled by sulcus (*red*) or gyrus (*blue*). **e** The corresponding inflated surface which has the same number of points with (**a**). **f** Map of the sulcus and gyrus feature on the inflated surface. **g** Second profile on a sulcus vertex. **h** Profile spokes labeled by sulcus or gyrus. **i** Cortical surface with the detected centers of three hinges (*yellow dots*)

was defined such that the z-axis was the average surface norm of three-hinge patch (Fig. 3a). Then, three hinge lines were extracted such that each hinge line was the gyral crest of the combination of any two hinges of three hinges (Fig. 3b). For consistent measurement and classification across three hinges and species, each hinge line was: first, projected to the x–y plane of the local coordinate system; second, rescaled such that the total length of the hinge line is 100 mm; third, re-sampled evenly into 50 nodes such that the distance between adjacent nodes along a hinge line is the same. Then, two sets of features were computed to quantitatively measure the morphology patterns of hinge lines as follows.

1. The average determinant of an orientation matrix O as a measurement of curvedness.

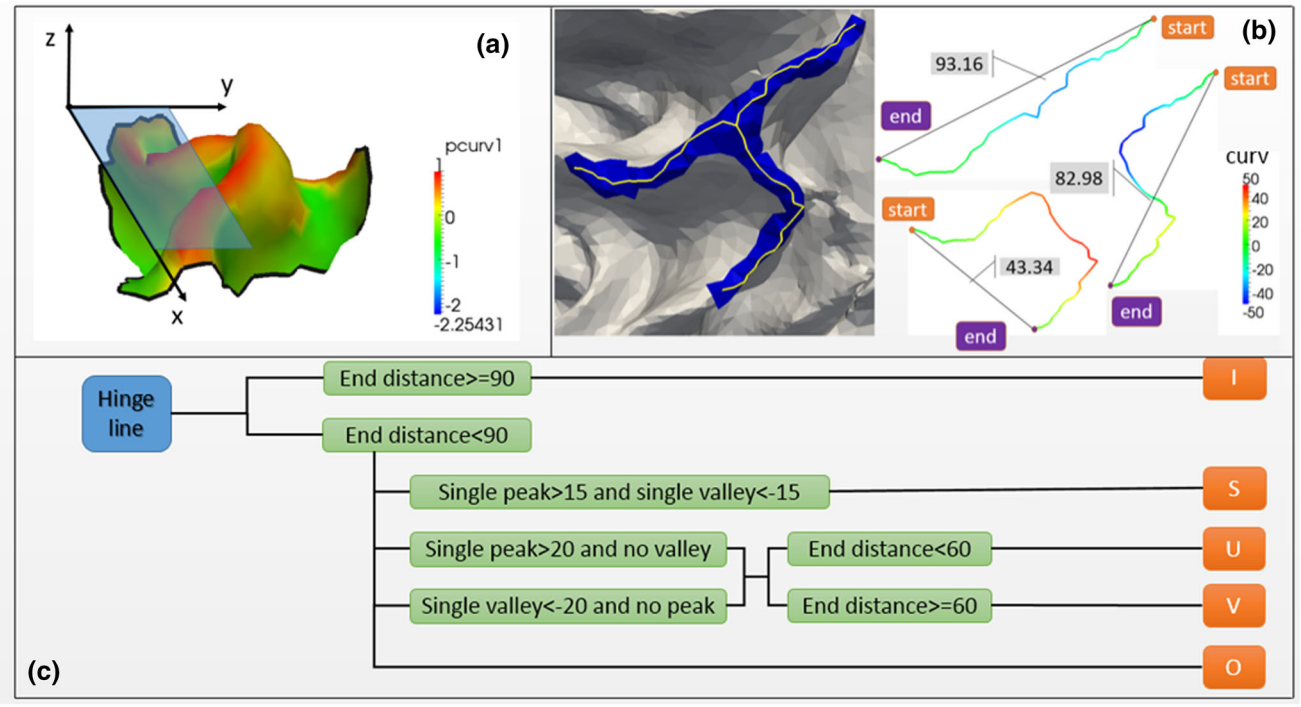

Fig. 3 Illustration of *morphology* descriptor and an example. **a** An example of gradient map of altitude in the local coordinate system of a patch. **b** Examples of decomposing a three-hinge gyrus into *hinge lines* and the *hinge line* morphology classification. The three hinges are of 'SUI' morphology patterns as the three *hinge lines* of it are '*S*', '*U*' and '*I*'. **c** Decision tree for *hinge line* classification

For a node v_i on the hinge line L, its curvedness c_i is defined as:

$$c_i = \frac{\sum_w^{j=1} \det(O(v_i, j, L))}{w} \quad (2)$$

where w is the maximum window width of the segment centered at v_i, $\det(O(v_i, j, L))$ is the determinant of the orientation matrix with span j. Denote (x_i, y_i) as the coordinate of vertex v_i, then

$$O(v_i, j, L) = \begin{bmatrix} 1 & x_{i-j} & y_{i-j} \\ 1 & x_i & y_i \\ 1 & x_{i+j} & y_{i+j} \end{bmatrix} \quad (3)$$

As shown in Fig. 3b, c_i reflects not only curvedness but also the direction that hinge line bends.

2. The Euclidean distance over the geodesic distance along the hinge line between the terminals of a hinge line as a measurement of its straightness.

Based on these two features, we can classify those hinge lines into different types (Fig. 3c). Since the length of the hinge line has been normalized to 100 mm, it is intuitive that the hinge line will be relatively straight if the Euclidean distance between the terminals is close to 100 mm, otherwise it will be relatively curved. Thus, empirically, if the Euclidean distance between terminals is larger than 90 mm, the hinge line will be taken as 'I' morphology pattern. For the rest of the ones, we then look into the curvedness measurements. If the hinge line only bends at the center of three hinges (only 1 extreme with absolute value larger than 20 in curvedness), it will be classified as either 'U' pattern or 'V'. The ones that have a wide-open terminals (Euclidean distance larger than 60) will be classified as 'V' pattern and the rest will be classified as 'U' pattern. For the hinge lines bending to the opposite directions on both sides of the cross point (two extremes in curvedness and one is larger than 15 and one is smaller than −15), they will be classified as 'S' morphology pattern. The rest ones that cannot be classified into four previously mentioned types were classified as other types represented by 'O'. The classification process can be summarized and solved by the decision tree shown in (Fig. 3c).

Since each three-hinge gyrus can be decomposed into three hinge lines, the morphology patterns of a three-hinge gyrus can be described by the combination of the sub-types of its hinge lines. We used the combination of letters of the hinge line sub-types to represent the combination pattern of three-hinge gyri. Taking the one in Fig. 3b, for example, 'SUI' indicates that the three-hinge gyri is composed of one 'U' pattern hinge line, one 'S' pattern hinge line and one 'I' pattern hinge line.

Results

By applying the computational approaches described in "Three-hinge gyral fold extraction" and "Morphology descriptor of three-hinge gyral fold" to the neuroimaging datasets listed in "Neuroimaging data and pre-processing", we visually and quantitatively assessed the consistency of three-hinge gyral locations ("Three-hinge gyral folds", "Commonly preserved three-hinge gyral folds", "Species-specific three-hinge gyral folds") and their folding pattern profiles ("Morphology analysis of three-hinge gyral fold") across human, chimpanzee, and macaque.

Three-hinge gyral folds

By applying the method proposed in "Three-hinge gyral fold extraction", initially three hinges were identified on reconstructed cortical surfaces. Then, the automatic results were visually inspected. The false-positive three-hinge folds were eliminated and the missing ones were manually added. In total, 85% automatically detected three hinges were accepted by visual inspection (precision) and 94% finally accepted three hinges were identified by proposed automatic approach (sensitivity). The precision and the sensitivity are similar across three species examined.

The average number of three hinges identified per subject within each species is listed in Table 1a. It is not surprising that the number of three hinges identified in human brain is 2.5 times more than the ones identified in chimpanzee brain and 7.8 times more than the ones identified in macaque brain. Intriguingly, though the number of three hinges linearly increased with the size of brain volume across these three species, further investigation did not show clear link between brain size and three-hinge numbers. As shown in Fig. 4, there is no clear correlation between three-hinge numbers and brain volume sizes within each species. The correlation coefficients between the brain volume size and the three-hinge numbers in human/chimpanzee/macaque brains are −0.10/0.49/−0.12, respectively.

All three hinges were aligned and visualized in the template space (Fig. 5). During visual inspection, we noticed that some three hinges could be consistently identified in the same anatomical regions across subjects. For instance, among most subjects, there were always three hinges on the joint of precentral gyrus and superior frontal gyrus. We defined such three hinges that retain in the same brain region across individuals with high confidence as anatomically consistent three hinges. Based on the spatial coherent and anatomical information, we identified 8 anatomically consistent three hinges in macaque brains, 12 anatomically consistent three hinges in chimpanzee brains, and 20 anatomically consistent three hinges in human brains. Those three hinges are highlighted by specific colors in Fig. 5.

Commonly preserved three-hinge gyral folds

Among the anatomically consistent three-hinge gyral folds, the ones located on the same anatomical area across species were identified as commonly preserved three-hinge gyral folds. In total, we identified six commonly preserved three-hinge gyral folds across three species of primate brains (those highlighted by black circles in Fig. 5). Our identified preserved three hinges are bilaterally located at the interface of same gyri across species including interface of superior frontal gyrus and precentral gyrus, interface of middle frontal gyrus and precentral gyrus, as well as interface of postcentral gyrus and superior parietal gyrus as shown in Fig. 6. These gyri are preserved and easily identified in macaque, chimpanzee and human brain. The consistencies of these commonly preserved three-hinge gyral folds are given in Table 1b. It should be noted that the

Table 1 The numbers of three-hinge gyral folds across primates and their distributions

	Macaque	Chimpanzee	Human
Number of subjects	20	16	64
(a) Average number of three hinges identified per subject			
Automatically identified three hinges	10.5	31.6	80.7
Correct three hinges identified automatically	8.9	28.1	67.3
Final three hinges after manual correction	9.5	29.3	74.2
(b) The percentage of *commonly* preserved three-hinge gyral folds identified in all subjects			
Right postCentral gyrus (rPoG)	95%	100%	96.88%
Middle right preCentral gyrus (rMPrG)	100%	87.5%	90.63%
Dorsal right preCentral gyrus (rDPrG)	95%	93.75%	93.75%
Left postCentral gyrus (lPoG)	100%	93.75%	96.88%
Middle left preCentral gyrus (lMPrG)	100%	100%	90.63%
Dorsal left preCentral gyrus (lDPrG)	100%	100%	92.19%

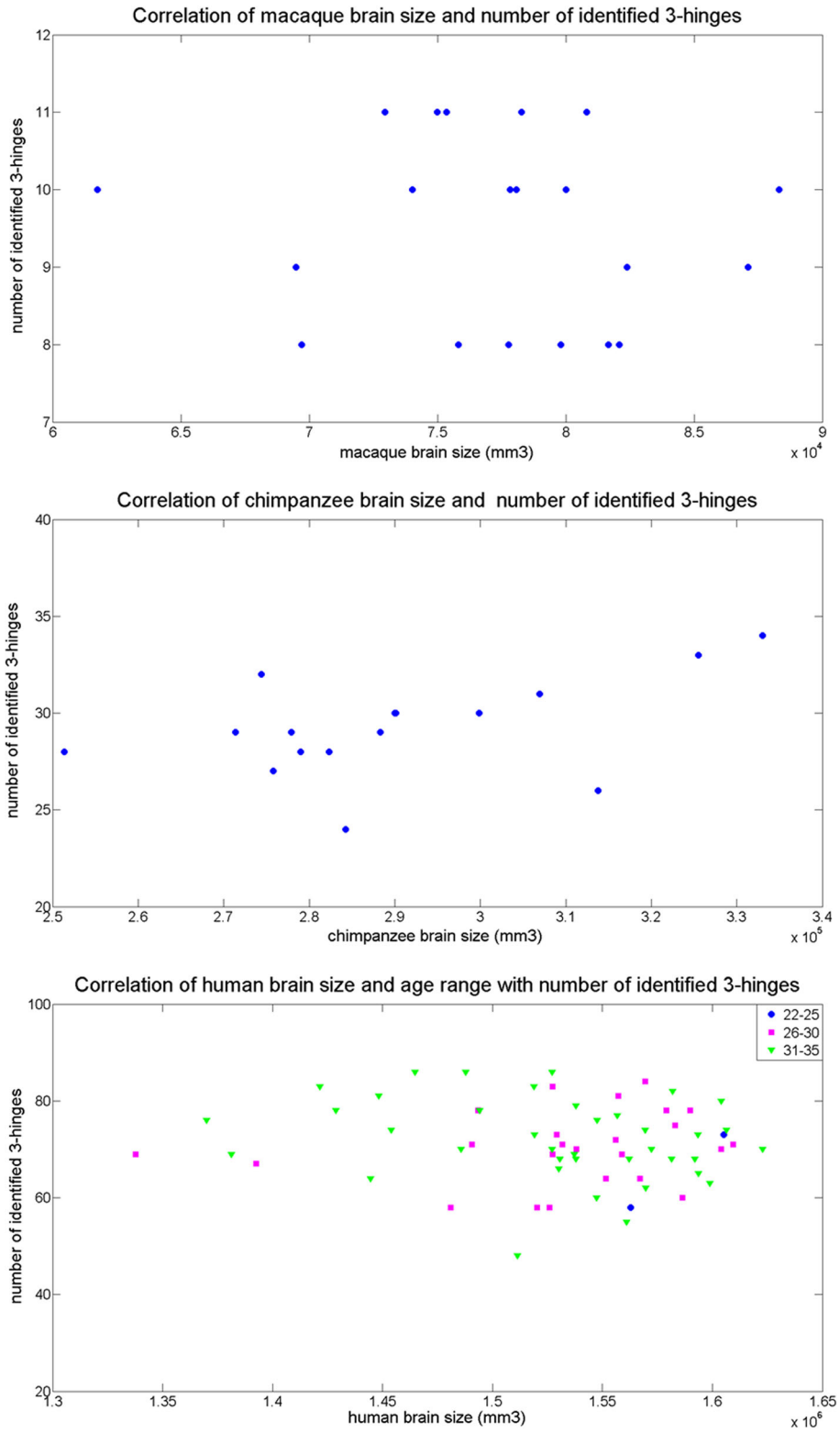

Fig. 4 The correlation of brain size and identified three-hinge numbers in three species. The *three graphs* from *top to bottom* are, respectively, associated with the correlation of macaque, chimpanzee and human brain size with their identified three-hinge numbers. Human subjects are categorized by age

six consistent three-hinge gyral folds are not necessarily found on the cortical surface of all subjects. The absences of some of the three-hinge gyral folds in certain subjects were attributed in part to the limitation of image quality and tissue segmentation accuracy, and/or by the normal variability between individuals.

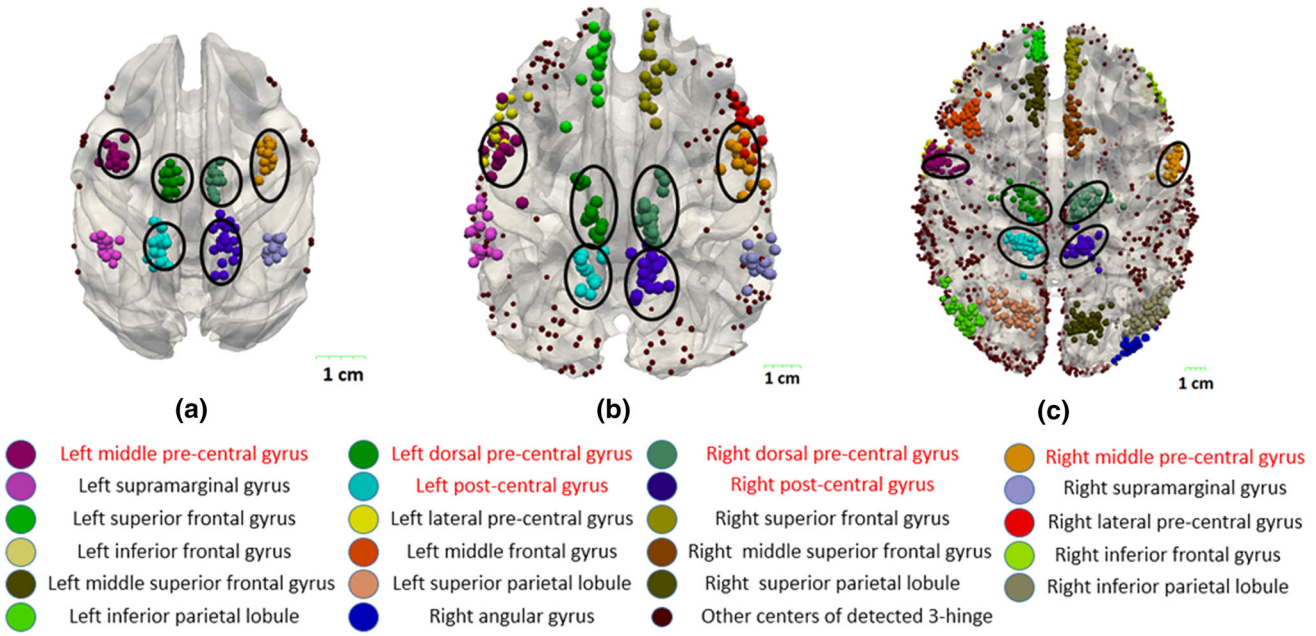

Fig. 5 Illustrations of all of the identified three-hinge gyral folds in the brains of three species (**a**–**c** macaque, chimpanzee and human, respectively). Each *sphere* represents a three-hinge gyral fold of a subject. All subjects in each species were linearly aligned to the space of randomly selected subject before visualization. The three-hinge gyral folds with correspondences were labeled in the *same colors*, as annotated at the *bottom*. The *same color* was assigned to the corresponding commonly preserved three hinges. These gyri in the *black circle* and shown in *red text* are commonly preserved three hinges

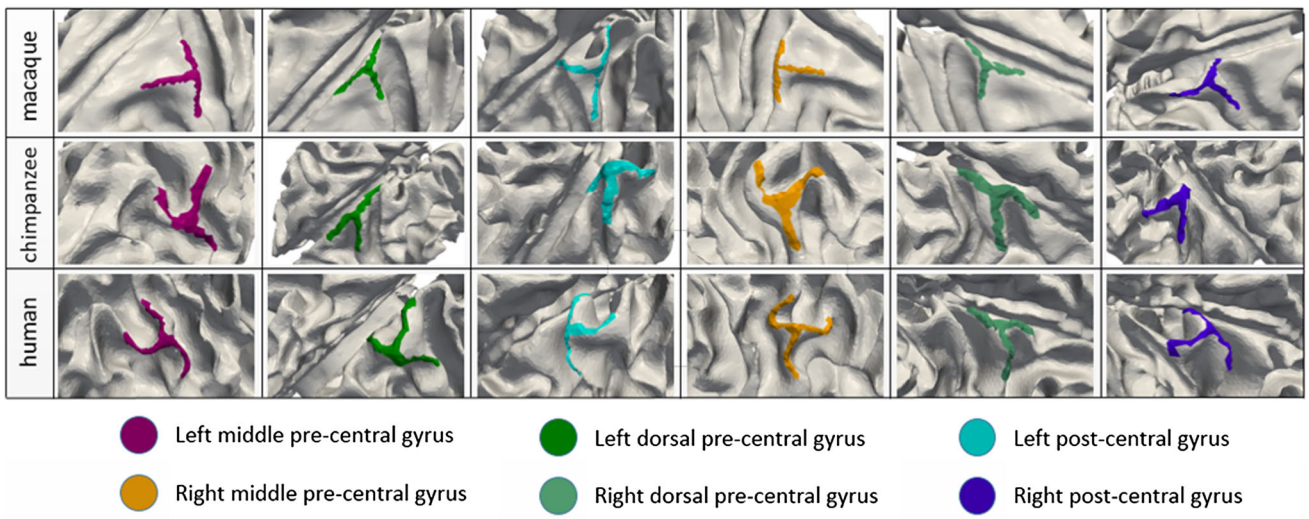

Fig. 6 The six consistent three-hinge gyral folds highlighted by *different colors* on example brains for each of three species, respectively

Species-specific three-hinge gyral folds

Besides those three-hinge gyri with commonly preserved consistency, as illustrated in Fig. 5, some other anatomically consistent three hinges were identified in specific species. In total, two anatomically consistent three hinges bilaterally located on supramarginal gyrus were consistently identified on macaque brain and chimpanzee brain only, four anatomically consistent three hinges were identified on both chimpanzee brain and human brain, and ten other anatomically consistent three hinges were only identified on human brain (Table 2).

Morphology analysis of three-hinge gyral fold

Using the approach proposed in "Morphology descriptor of three-hinge gyral fold", the hinge lines were extracted from three hinges and classified based on its morphological

Table 2 The numbers of species-specific three-hinge gyral folds across primates and their distributions

	Macaque	Chimpanzee	Human
Number of subjects	20	16	64
Rate of the subjects detected species-specific three hinges in all subjects			
Right supramarginal gyrus	100%	100%	31.25%
Left supramarginal gyrus	100%	93.75%	39.06%
Right lateral precentral gyrus	25%	100%	96.88%
Left lateral precentral gyrus	30%	100%	96.88%
Right superior frontal gyrus	0%	100%	95.31%
Left superior frontal gyrus	5%	93.75%	92.19%
Left middle frontal gyrus	0%	12.5%	93.75%
Right middle superior frontal gyrus	0%	0%	90.63%
Left inferior frontal gyrus	15%	12.5%	93.75%
Right inferior frontal gyrus	25%	6.25%	98.44%
Left middle superior frontal gyrus	0%	0%	96.88%
Left superior parietal lobule	0%	18.75%	98.44%
Right superior parietal lobule	0%	12.5%	95.31%
Right inferior parietal lobule	0%	0%	96.88%
Left inferior parietal lobule	0%	0%	96.88%
Right angular gyrus	0%	0%	92.19%

Table 3 The percentage of each morphology descriptor appears at center type gyrus

	Macaque					Chimpanzee					Human				
	V (%)	I (%)	U (%)	S (%)	O (%)	V (%)	I (%)	U (%)	S (%)	O (%)	V (%)	I (%)	U (%)	S (%)	O (%)
rMPrG	60	28	3	0	8	31	27	13	8	21	16	13	26	21	24
rDPrG	78	18	2	0	2	52	27	6	8	6	32	21	12	15	20
rPoG	60	22	3	7	8	50	21	15	6	8	22	19	23	14	22
lMPrG	60	32	5	0	3	33	25	10	15	17	13	16	27	16	28
lDPrG	72	25	3	0	0	65	19	4	2	10	25	25	15	15	21
lPoG	70	23	2	2	3	48	15	23	4	10	24	20	21	9	26
Commonly preserved	67	25	3	1	4	47	22	12	7	12	22	19	21	15	23
All	53	30	7	3	8	39	22	15	9	14	20	18	19	14	27

feature. Specifically, we compared the folding composition of three hinges across species (Table 3). In macaque's brain, the relatively straight *patterns* 'I' (30%) and 'V' (53%) are the most dominant morphology patterns among five morphology patterns. In chimpanzees and human brain, though there is still a considerable amount of 'I' and 'V' morphology patterns, the percentage of more convoluted morphology patterns such as 'U' and 'S' increased significantly. Moreover, the most dominant morphology pattern in human brain is the 'O' (27%) pattern which cannot be classified into the four basic morphology patterns we designated.

We then examined the pattern of the combination of hinge line morphology patterns of three hinges. The total number of different combinations in three species was counted and is shown in Fig. 7. Again, the relatively simple *morphology pattern* combinations 'VVV' (16.25%) and 'VVI' (40.625%) dominate in macaque brain. In chimpanzee brain, there are more different types of combinations, while the major combination includes the relatively straight morphology pattern 'VVI' (13.54%), and more convoluted pattern 'VIU' (11.46%) and 'VIO' (9.9%). However, the pattern is more diverse in human brain. Not only are there more combinations of morphology patterns, but also these combinations are evenly distributed. Among them, the convoluted morphology patterns 'VIO' (8.13%) and 'IUS' (8.13%) dominate. Examples of different morphology pattern combinations in different species on left dorsal precentral gyrus are shown in Fig. 8. It can be seen that even the three-hinge gyral folds located at the same area have very different morphology patterns.

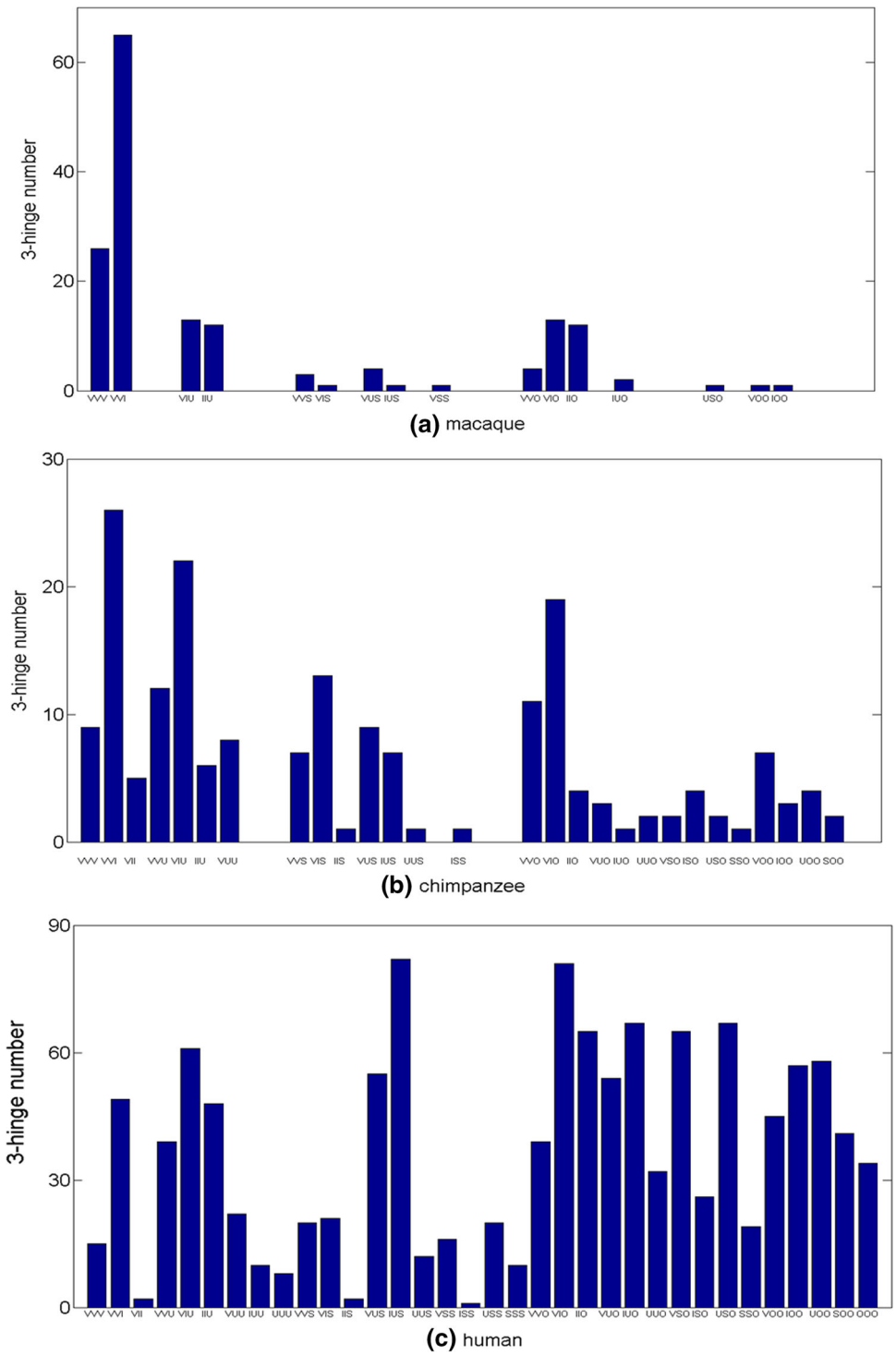

Fig. 7 Histogram of three-hinge morphology pattern combinations in each species. Each *bar* represents a specific combination that appears and the combinations were ordered such that the ones on the *right* is more convoluted than the ones on the *left*

Discussion and conclusion

In this paper, we introduced, evaluated, and applied a novel computational framework to quantify cortical gyral folds in three primate species—macaque, chimpanzee, and human being. Specifically, our analysis focused on the joint area of gyri—three-hinge gyral folds. A computational framework has been proposed to automatically detect three hinges on reconstructed WM cortical surface. Then, the three hinges that were group-wise and anatomically consistent within or across species were identified. Based on a newly proposed scheme of *morphology* classification, the morphology pattern of identified three hinges were further analyzed and compared across species.

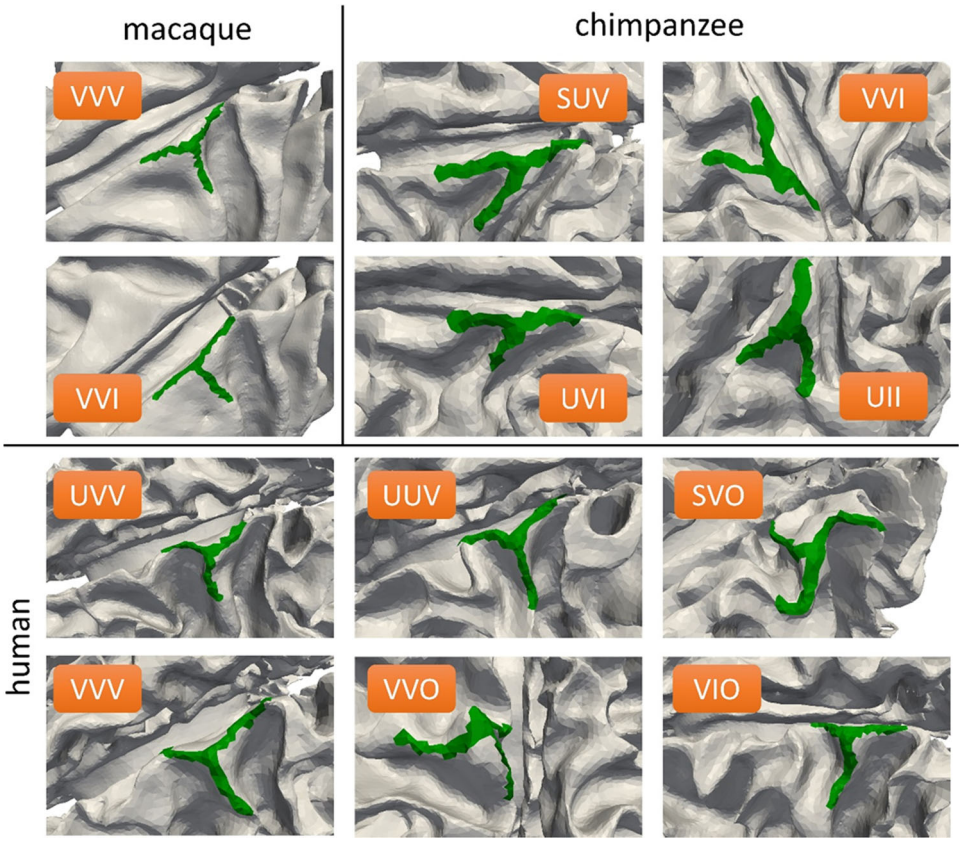

Fig. 8 The example of different morphology pattern appeared at left dorsal precentral gyri, which is a consistent three-hinge gyral fold. There are two main morphology pattern combinations in macaque and four in chimpanzee, but there are more than six appeared in human brain

On average, human brain has more three hinges than chimpanzee and macaque brain. Based on spatial and anatomical locations of three hinges across subjects, anatomically consistent three hinges were identified. Again, more anatomically consistent three hinges were identified in human brain. However, the consistent three hinges in human brain only took a small portion of the three hinges totally identified in comparison with chimpanzee and macaque suggesting higher variability of cortical folds between human individuals. For example, we can find about 74 three hinges in human cortical surface on average, while only 20 of them are consistent across individuals. In macaque brain, there are only 9.5 three hinges identified on average and 8 of them were shown to be anatomically consistent across individuals.

By comparing the anatomically consistent three hinges across species, both commonly preserved three hinges and species-specific three hinges were identified. Notably, all of the six preserved three hinges are identified on precentral and post-central gyri. This observation agrees with the current neuroscience knowledge that the precentral gyrus and the post-central gyrus are among the most well-preserved gyrus across mammalians (Roland and Zilles 1996). Despite those commonly preserved gyral folds, we also identified species-specific gyral folds that can only be consistently found in one or two primate species we analyzed. Specifically, we found 14 species-specific gyral folds in human brain, 6 in chimpanzee brain, and 2 in macaque brain. Most of these three-hinge gyral folds are either on frontal lobe or on parietal lobe. However, it is intriguing that even though human brain has more three hinges than the other two primates, three hinges located on supramarginal gyrus can only be identified in macaque and chimpanzee brain consistently. On the other hand, four other three-hinge gyral folds bilaterally located on parietal lobule were only identified in human brain. As for frontal lobe, two three-hinge gyral folds were consistently identified in chimpanzee brain and human brain at the superior frontal gyrus, while human brain has four more anatomically consistent three hinges than chimpanzee. Moreover, though we can identify anatomically consistent three hinges that are only common between macaque and chimpanzee brain or between chimpanzee and human brain, there is no such overlapping between macaque and human brain. It is possible that such anatomical specialization is related to the functional specialization of brains across species (Van Essen et al. 2001; Van Essen 2002; Rilling et al. 2008; Passingham 2009). Further experiments on the brain activity in the corresponding area are needed to validate this hypothesis. If those anatomically consistent three hinges also preserve functional consistency across subjects, they can be further applied to identify anatomical

and functional correspondence across species and can be employed as important landmarks for across-species registration.

In addition to the increased variability of spatial distribution of three hinges, the variability and the complexity of gyral morphology patterns in human neocortex are also higher in comparison with the macaque and chimpanzee brains. To quantify the shape complexity, we empirically defined five basic types of the gyral crest line and use the combination of these five basic patterns to describe the morphology of three-hinge gyral folds. Our analysis showed that the gyral crest of macaque brain is relatively straight and the three-hinge gyral folds are composed of a few simple patterns. Meanwhile, human brain cortical morphology is the most complicated given that it is composed of highly diverse patterns. However, it should be noted that this heuristic three-hinge morphology classification approach has limited description power. It is purely designed based on our observations. When applied to quantify complicated human brain morphology, some patterns cannot be described accurately. For example, in human brain, 27% gyral crests cannot be classified by the four simple patterns we defined and thus were classified as "other type (O)". Moreover, since the classification is based on five basic types, the problem could be oversimplified and some sub-types of three-hinge morphology are overlooked. For a more comprehensive classification of three-hinge gyral fold morphology, data-driven approaches should be designed in the future to generate clusters of three-hinge patterns.

Nevertheless, the proposed meso-scale folding pattern descriptor will also shed light on brain developmental studies. So far, there are numerous works reporting the hypothesized cortical folding regulators including the roles of radial growth (Smart and McSherry 1986a, b), internal tension in neuronal fibers (Van Essen 1997), and differential expansion of the cortex (Richman et al. 1975). These hypotheses have been quantitatively evaluated by the direct measurements of brain morphological parameters based on biomechanical/developmental data and the computational simulation of mathematical models (Van Essen 1997; Hilgetag and Barbas 2005, 2006; Toro and Burnod 2005; Toro 2012; Bayly et al. 2014; Tallinen et al. 2016). Although plausible in one way or another, most studies only investigated possible mechanisms by focusing on basic gyro-sulcal pattern in 2D space. Very few studies in the literature are found to report an effective way to infer possible reasons underlying the overall landscapes of folding in 3D space. The models with realistic initial morphology are needed (Nie et al. 2010; Tallinen et al. 2016). The three-hinge gyral folding pattern examined in this paper is defined in 3D space and well preserved across subjects and multiple species. However, its emerging process as well as its driven mechanical factors has been rarely explored in the literature so far. From the developmental perspective, all the six commonly preserved three hinges are around central sulcus which emerges at 21 weeks in human fetus when brain is relatively flat (Nishikuni and Ribas 2013). Since the brains of human, chimpanzee, and macaque are in similar flat shape in this stage, we hypothesize that the convolution process of these three hinges follow similar rules across species.

In future works, further investigations are needed to unveil the mechanisms that regulate the development of three hinges as well as their functional roles. Although the identified commonly preserved three-hinge gyral folds are consistent in anatomical location, significant differences on their folding morphology patterns were also identified between species which cast doubts on whether these three-hinge gyral folds show structural and functional correspondence across species. To clarify such doubt, it requires further examination via other approaches such as microstructure of neuroanatomy using morphological study (Buxhoeveden et al. 2001), functional activation with functional magnetic resonance imaging (Orban et al. 2004), or joint analysis on axonal connectivity using diffusion tensor image (Chen et al. 2013; Zhang et al. 2013). In addition, the three-hinge pattern examined in this paper missed a lot of information of cortical anatomy. A unified framework for further joint analysis of different cortical area (gyral and sulcus), wiring pattern, and brain functional activity is needed to fully investigate brain differences and its mechanism across species.

Acknowledgements T Liu was supported by the NIH Career Award EB006878 (2007–2012), NIH R01 HL087923-03S2 (2010–2012), NIH R01 DA033393 (2012–2017), NIH R01 AG-042599 (2013–2018), NSF CAREER Award IIS-1149260 (2012-2017), NSF CBET-1302089 (2013–2016), NSF BCS-1439051 (2014–2017) and NSF DBI-1564736 (2016–2019). T Zhang was supported by NSFC 31500798, the fundamental research funds for the central universities.

References

Barkovich AJ (2010) Current concepts of polymicrogyria. Neuroradiology 52:479–487

Barton RA (2006) Primate brain evolution: integrating comparative, neurophysiological, and ethological data. Evol Anthropol Issues News Rev 15:224–236

Bayly PV, Taber LA, Kroenke CD (2014) Mechanical forces in cerebral cortical folding: a review of measurements and models. J Mech Behav Biomed Mater 29:568–581

Bullmore E, Sporns O (2009) Complex brain networks: graph theoretical analysis of structural and functional systems. Nat Rev Neurosci 10:186–198

Buxhoeveden DP, Switala AE, Roy E, Litaker M, Casanova MF (2001) Morphological differences between minicolumns in human and nonhuman primate cortex. Am J Phys Anthropol 115:361–371

Chen H, Zhang T, Guo L, Li K, Yu X, Li L, Hu X, Han J, Hu X, Liu T (2013) Coevolution of gyral folding and structural connection patterns in primate brains. Cereb Cortex 23:1208–1217

Chen H, Yu X, Jiang X, Li K, Li L, Hu X, Han J, Guo L, Hu X, Liu T (2014) Evolutionarily-preserved consistent gyral folding patterns across primate brains. In: ISBI. IEEE. p 1218–1221

Dubois J, Benders M, Borradori-Tolsa C, Cachia A, Lazeyras F, Leuchter HV, Sizonenko SV, Warfield SK, Mangin JF, Hüppi PS (2008) Primary cortical folding in the human newborn: an early marker of later functional development. Brain A J Neurol 131:2028–2041

Dunbar RIM, Shultz S (2007) Evolution in the social brain. Science 317:1344–1347

Fischl B, Sereno MI, Dale AM (1999) Cortical surface-based analysis: II: inflation, flattening, and a surface-based coordinate system. Neuroimage 9:195–207

Fischl B, Rajendran N, Busa E, Augustinack J, Hinds O, Yeo BTT, Mohlberg H, Amunts K, Zilles K (2008) Cortical folding patterns and predicting cytoarchitecture. Cereb Cortex 18:1973–1980

Giedd JN, Rapoport JL (2010) Structural MRI of pediatric brain development: What have we learned and where are we going? Neuron 67:728–734

Greicius MD, Krasnow B, Reiss AL, Menon V (2003) Functional connectivity in the resting brain: a network analysis of the default mode hypothesis. Proc Natl Acad Sci USA 100:253–258

Hardan AY, Jou RJ, Keshavan MS, Varma R, Minshew NJ (2004) Increased frontal cortical folding in autism: a preliminary MRI study. Psychiatry Res 131:263–268

Harris JM, Whalley H, Yates S, Miller P, Johnstone EC, Lawrie SM (2004) Abnormal cortical folding in high-risk individuals: a predictor of the development of schizophrenia? Biol Psychiatry 56:182–189

Heimann T, Meinzer H-P (2009) Statistical shape models for 3D medical image segmentation: a review. Med Image Anal 13:543–563

Hilgetag CC, Barbas H (2005) Developmental mechanics of the primate cerebral cortex. Anat Embryol (Berl) 210:411–417

Hilgetag CC, Barbas H (2006) Role of Mechanical Factors in the Morphology of the Primate Cerebral Cortex. PLoS Comput Biol 2:e22

Honey CJ, Sporns O, Cammoun L, Gigandet X, Thiran JP, Meuli R, Hagmann P (2009) Predicting human resting-state functional connectivity from structural connectivity. Proc Natl Acad Sci USA 106:2035–2040

Honey CJ, Thivierge J-P, Sporns O (2010) Can structure predict function in the human brain? Neuroimage 52:766–776

Jenkinson M, Smith S (2001) A global optimisation method for robust affine registration of brain images. Med Image Anal 5:143–156

Jenkinson M, Bannister P, Brady M, Smith S (2002) Improved optimization for the robust and accurate linear registration and motion correction of brain images. Neuroimage 17:825–841

Jenkinson M, Beckmann CF, Behrens TEJ, Woolrich MW, Smith SM (2012) FSL. Neuroimage 62:782–790

King R, Brown B, Hwang MSH, Jeon T, George AT (2010) Fractal dimension analysis of the cortical ribbon in mild Alzheimer's disease. Neuroimage 53:471–479

Landrieu P, Husson B, Pariente D, Lacroix C (1998) MRI-neuropathological correlations in type 1 lissencephaly. Neuroradiology 40:173–176

Li K, Guo L, Li G, Nie J, Faraco C, Cui G, Zhao Q, Miller LS, Liu T (2010) Gyral folding pattern analysis via surface profiling. Neuroimage 52:1202–1214

Li G, Wang L, Shi F, Lyall AE, Lin W, Gilmore JH, Shen D (2014) Mapping longitudinal development of local cortical gyrification in infants from birth to 2 years of age. J Neurosci 34:4228–4238

Liu T (2011) A few thoughts on brain ROIs. Brain Imaging Behav 5:189–202

Liu T, Nie J, Tarokh A, Guo L, Wong STC (2008) Reconstruction of central cortical surface from brain MRI images: method and application. Neuroimage 40:991–1002

Luders E, Thompson PM, Narr KL, Toga AW, Jancke L, Gaser C (2006) A curvature-based approach to estimate local gyrification on the cortical surface. Neuroimage 29:1224–1230

MacLeod CE, Zilles K, Zilles K, Schleicher A, Rilling JK, Gibson KR (2003) Expansion of the neocerebellum in Hominoidea. J Hum Evol 44:401–429

Mantini D, Gerits A, Nelissen K, Durand J-B, Joly O, Simone L, Sawamura H, Wardak C, Orban GA, Buckner RL, Vanduffel W (2011) Default mode of brain function in monkeys. J Neurosci 31:12954–12962

Marquardt D (1963) An algorithm for least-squares estimation of nonlinear parameters. J Soc Ind Appl Math 11:431–441

Neal J, Takahashi M, Silva M, Tiao G, Walsh CA, Sheen VL (2007) Insights into the gyrification of developing ferret brain by magnetic resonance imaging. J Anat 210:66–77

Nie J, Guo L, Li G, Faraco C, Stephen Miller L, Liu T (2010) A computational model of cerebral cortex folding. J Theor Biol 264:467–478

Nie J, Guo L, Li K, Wang Y, Chen G, Li L, Chen H, Deng F, Jiang X, Zhang T, Huang L, Faraco C, Zhang D, Guo C, Yap P-T, Hu X, Li G, Lv J, Yuan Y, Zhu D, Han J, Sabatinelli D, Zhao Q, Miller LS, Xu B, Shen P, Platt S, Shen D, Hu X, Liu T (2012) Axonal fiber terminations concentrate on gyri. Cereb Cortex 22:2831–2839

Nishikuni K, Ribas GC (2013) Study of fetal and postnatal morphological development of the brain sulci: laboratory investigation. J Neurosurg: Pediatr 11(1):1–11

Nordahl CW, Dierker D, Mostafavi I, Schumann CM, Rivera SM, Amaral DG, Van Essen DC (2007) Cortical folding abnormalities in autism revealed by surface-based morphometry. J Neurosci 27:11725–11735

Orban GA, Van Essen D, Vanduffel W (2004) Comparative mapping of higher visual areas in monkeys and humans. Trends Cogn Sci 8:315–324

Passingham R (2009) How good is the macaque monkey model of the human brain? Curr Opin Neurobiol 19:6–11

Pereira JB, Ibarretxe-Bilbao N, Marti MJ, Compta Y, Junqué C, Bargallo N, Tolosa E (2012) Assessment of cortical degeneration in patients with Parkinson's disease by voxel-based morphometry, cortical folding, and cortical thickness. Hum Brain Mapp 33:2521–2534

Richman DP, Stewart RM, Hutchinson JW, Caviness VS (1975) Mechanical model of brain convolutional development. Science 189:18–21

Rilling JK (2006) Human and nonhuman primate brains: are they allometrically scaled versions of the same design? Evol Anthropol Issues. News Rev 15:65–77

Rilling JK, Insel TR (1999) The primate neocortex in comparative perspective using magnetic resonance imaging. J Hum Evol 37:191–223

Rilling JK, Seligman RA (2002) A quantitative morphometric comparative analysis of the primate temporal lobe. J Hum Evol 42:505–533

Rilling JK, Glasser MF, Preuss TM, Ma X, Zhao T, Hu X, Behrens TEJ (2008) The evolution of the arcuate fasciculus revealed with comparative DTI. Nat Neurosci 11:426–428

Roland PE, Zilles K (1996) Functions and structures of the motor cortices in humans. Curr Opin Neurobiol 6:773–781

Ronan L, Voets NL, Rua C, Alexanderbloch A, Hough M, Mackay CE, Crow TJ, James AC, Giedd JN, Fletcher PC (2013) Differential tangential expansion as a mechanism for cortical gyrification. Cereb Cortex 24:2219

Rosas HD, Liu AK, Hersch S, Glessner M, Ferrante RJ, Salat DH, van der Kouwe A, Jenkins BG, Dale AM, Fischl B (2002) Regional and progressive thinning of the cortical ribbon in Huntington's disease. Neurology 58:695–701

Sallet PC, Elkis H, Alves TM, Oliveira JR, Sassi E, Campi de Castro C, Busatto GF, Gattaz WF (2003) Reduced cortical folding in schizophrenia: an MRI morphometric study. Am J Psychiatry 160:1606–1613

Schoenemann PT (2006) Evolution of the size and functional areas of the human brain. Annu Rev Anthropol 35:379–406

Smaers JB, Soligo C (2013) Brain reorganization, not relative brain size, primarily characterizes anthropoid brain evolution. Proc Biol Sci 280:20130269

Smart IH, McSherry GM (1986a) Gyrus formation in the cerebral cortex in the ferret. I. Description of the external changes. J Anat 146:141–152

Smart IH, McSherry GM (1986b) Gyrus formation in the cerebral cortex of the ferret. II. Description of the internal histological changes. J Anat 147:27–43

Tallinen T, Chung JY, Rousseau F, Girard N, Lefevre J, Mahadevan L (2016) On the growth and form of cortical convolutions. Nat Phys 12:588–593

Thompson PM, Hayashi KM, Sowell ER, Gogtay N, Giedd JN, Rapoport JL, de Zubicaray GI, Janke AL, Rose SE, Semple J, Doddrell DM, Wang Y, van Erp TGM, Cannon TD, Toga AW (2004) Mapping cortical change in Alzheimer's disease, brain development, and schizophrenia. Neuroimage 23(Suppl):S2–S18

Toro R (2012) On the Possible Shapes of the Brain. Evol Biol 39:600–612

Toro R, Burnod Y (2005) A morphogenetic model for the development of cortical convolutions. Cereb Cortex 15:1900–1913

Tortori-Donati P, Rossi A, Biancheri R (2005) Brain Malformations. Springer, Berlin Heidelberg

Van Essen DC (1997) A tension-based theory of morphogenesis and compact wiring in the central nervous system. Nature 385:313

Van Essen DC (2002) Surface-based atlases of cerebellar cortex in the human, macaque, and mouse. Ann N Y Acad Sci 978:468–479

Van Essen DC, Lewis JW, Drury HA, Hadjikhani N, Tootell RBH, Bakircioglu M, Miller MI (2001) Mapping visual cortex in monkeys and humans using surface-based atlases. Vision Res 41:1359–1378

Van Essen DC, Ugurbil K, Auerbach E, Barch D, Behrens TEJ, Bucholz R, Chang A, Chen L, Corbetta M, Curtiss SW, Della Penna S, Feinberg D, Glasser MF, Harel N, Heath AC, Larson-Prior L, Marcus D, Michalareas G, Moeller S, Oostenveld R, Petersen SE, Prior F, Schlaggar BL, Smith SM, Snyder AZ, Xu J, Yacoub E (2012) The human connectome project: a data acquisition perspective. Neuroimage 62:2222–2231

Welker W (1990) Why does cerebral cortex fissure and fold?. A review of determinants of gyri and sulci, Cereb Cortex, p 8

Yeo BTT, Yu P, Grant PE, Fischl B, Golland P (2008) Shape Analysis with Overcomplete Spherical Wavelets. MICCAI LNCS Lect Notes Comput Sci 5241:468–476

Yu P, Han X, Ségonne F, Pienaar R, Buckner RL, Golland P, Grant PE, Fischl B (2006) Cortical Surface Shape Analysis Based on Spherical Wavelet Transformation. Conf Comput Vis Pattern Recognit Workshops

Yu X, Chen H, Zhang T, Hu X, Guo L, Liu T (2013) Joint analysis of gyral folding and fiber shape patterns. In: ISBI. IEEE. p 85–88

Zhang D, Guo L, Zhu D, Li K, Li L, Chen H, Zhao Q, Hu X, Liu T (2013) Diffusion tensor imaging reveals evolution of primate brain architectures. Brain Struct Funct 218:1429–1450

Zilles K, Armstrong E, Schleicher A, Kretschmann H-J (1988) The human pattern of gyrification in the cerebral cortex. Anat Embryol (Berl) 179:173–179